Fifth-Order Raman Spectroscopy of Liquid Benzene: Experiment and Theory†

C. J. Milne,‡ Y. L. Li,‡ T. l. C. Jansen,§ L. Huang,‡ and R. J. D. Miller*,‡

Departments of Chemistry and Physics, and the Institute for Optical Sciences, University of Toronto, 80 St. George Street, Toronto, Ontario M5S3H6, Canada, and Institute for Theoretical Physics and Materials Science Centre, University of Groningen, Nijenborgh 4, 9747 AG Groningen, The Netherlands

Received: April 3, 2006; In Final Form: July 12, 2006

The heterodyned fifth-order Raman response of liquid benzene has been measured and characterized by exploiting the passive-phase stabilization of diffractive optics. This result builds on our previous work with liquid carbon disulfide and extends the spectroscopy to a new liquid for the first time. The all-parallel and Dutch Cross polarization tensor elements are presented for both the experimental results and a finite-field molecular dynamics simulation. The overall response characteristics are similar to those of liquid carbon disulfide: a complete lack of signal along the pump delay, an elongated signal along the probe delay, and a short-lived signal along the time diagonal. Of particular interest is the change in phase between the nuclear and electronic response along the probe delay and diagonal which is not seen in CS_2. Good agreement is achieved between the experiment and the finite-field molecular dynamics simulation. The measurement of the low-frequency Raman two-time delay correlation function indicates the intermolecular modes of liquid benzene to be primarily homogeneously broadened and that the liquid loses its nuclear rephasing ability within 300 fs. This rapid loss of nuclear correlations indicates a lack of modal character in the low-frequency motions of liquid benzene. This result is a validation of the general nature of the technique and represents an important step forward with respect to the use of nonlinear spectroscopy to directly access information on the anharmonic motions of liquids.

1. Introduction

Fifth-order Raman spectroscopy is unique in its ability to distinguish between broadening mechanisms in the low-frequency modes of liquids.[1] This information content is crucial to understanding how intermolecular forces affect liquid dynamics. The observable in this experiment provides a sensitive probe of the intermolecular potentials used to model liquid dynamics. It effectively provides a direct measurement of the anharmonic contributions to the potential energy surface upon which many chemical and biochemical reactions take place. The importance of this information can be exemplified by considering how hydrogen bonding in water influences the structure of a protein and thus its function. A long-term goal of this research is to apply this spectroscopy to highly hydrogen-bonded liquids to directly access information on the many body potential and dynamics of hydrogen-bond networks. Fifth-order spectroscopy provides a new window on this problem, as there is no distinct spectral feature of liquids to distinguish different dynamical processes. The intermolecular spectrum (<500 cm^{-1}) is generally a featureless profile with a very similar spectrum for many liquids. The dynamics of the liquid can range from effectively static, slowly evolving structures in the inhomogeneous limit all the way through to quickly changing, homogeneously broadened dynamical systems within the time scale appropriate to the spectral line shape. These two extremes can produce the same broad low-frequency line shape, making it impossible to distinguish between inhomogeneous or homogeneous broadening mechanisms by measuring the one-dimensional spectrum of the liquid. The information content in the single time-delay, third-order nonlinear experiment is identical to that of the single frequency spectral measurement.[2] The solution is to use higher-order methods in which a second time variable is introduced that provides a means of accessing the time evolution of the bath. The lowest-order nonlinear interaction to give such two-dimensional spectroscopic information is fifth-order.

The importance of two-dimensional spectroscopic approaches has long been appreciated in NMR as a means to dissect congested spectra to measure spin coupling between nuclei, allowing a more complete picture of the molecular environment and structure to be developed. Experiments such as NMR's spin echo and visible spectroscopy's photon echo have enabled the differentiation between broadening mechanisms over a wide range of time scales and spectral regions.[3] Within the low-frequency range pertinent to intermolecular motions, the most viable method of preparing the relevant coherences is based on Raman processes. At this level of field interaction, the corresponding Raman echo is formally a $\chi^{(7)}$ nonlinear experiment.[4,5] The experiment involves three time-separated pump pulse pairs, each of which excites a Raman transition in the system of interest, followed by a probe pulse to sample the residual coherence. This experiment is normally discussed in the context of intramolecular vibrations and coupling to the surrounding bath. In analyzing this nonlinear interaction with respect to directly probing the bath dynamics, Tanimura and Mukamel discovered a lower-order $\chi^{(5)}$ rephasing pathway that is particularly relevant to low-frequency liquid modes and enables the distinction to be made between the various broadening mechanisms.[1] The rephasing process leading to an echo-like response at fifth-order involves a two-quantum transition to a Raman overtone and as such provides direct information on the

† Part of the special issue "Charles B. Harris Festschrift".
‡ University of Toronto.
§ University of Groningen.

10.1021/jp062063v CCC: $33.50
Published on Web 09/23/2006

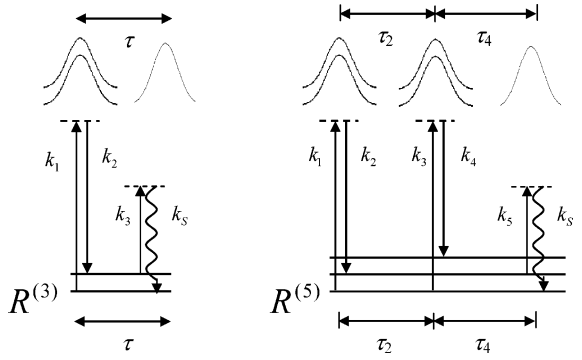

Figure 1. Pulse sequence (top) and energy level diagram (bottom) for third-order (left) and fifth-order (right) Raman spectroscopy. The electronically nonresonant third-order spectroscopy consists of a pair of time-coincident pump pulses ($\mathbf{k_1}$, $\mathbf{k_2}$) followed by a probe pulse ($\mathbf{k_3}$) after a time delay, τ. The fifth-order electronically nonresonant spectroscopy consists of two pump pulse pairs ($\mathbf{k_1}$, $\mathbf{k_2}$, and $\mathbf{k_3}$, $\mathbf{k_4}$) separated by a time delay, τ_2, followed by a probe pulse ($\mathbf{k_5}$) after a second time delay, τ_4. In both cases, a signal field ($\mathbf{k_s}$) is generated by the scattering of the probe off the pump-induced grating in the sample.

anharmonic motion of liquids that is central to understanding the liquid state.

The general methodology of this experiment is based on an extension of the optical Kerr effect, third-order Raman spectroscopy.[6,7] In this spectroscopy, two time-coincident electronically nonresonant pump pulses induce a Raman coherence between the ground and excited states of a low-frequency mode in the liquid. After some time delay, a probe pulse scatters off this coherence, generating the signal in the phase-matching direction $\mathbf{k_s} = (\mathbf{k_1} - \mathbf{k_2}) + \mathbf{k_3}$ (see Figure 1). As discussed, it is not possible to distinguish homogeneous from inhomogeneous line shape contributions from this single time variable spectroscopy. To access a second time variable, one needs a second pair of pulses, as shown in Figure 1. This second pulse pair transfers the Raman coherence to a superposition state involving a two-quantum transition. Within a harmonic oscillator approximation, the induced polarizations between the first and second excited states of the bath modes have exactly the same frequency distribution but there is a sign change in the polarization between the $0-1$ and $1-2$ coherences. This effect results in a 180° phase shift in the sample polarization for these field interactions which refocuses the inhomogeneous contributions to the line shapes and generates an echo signal. A probe pulse is then scattered off the induced polarization to probe the bath dynamics. The five input fields make this induced polarization a fifth-order interaction characterized by the $\chi^{(5)}$ nuclear susceptibility. The relative time delay between excitation pulse pairs is labeled τ_2, while the relative time delay between the probe pulse and the first excitation pulse pair is labeled τ_4. When inhomogeneous contributions to the line shape are present, the second coherence will cause a rephasing of the first coherence when $\tau_2 = \tau_4$, resulting in an echo-like signal analogous to photon echo spectroscopy.[3,8] The signal generated meets the phase-matching requirements $\mathbf{k_s} = (\mathbf{k_1} - \mathbf{k_2}) - (\mathbf{k_3} - \mathbf{k_4}) + \mathbf{k_5}$; in a non-collinear phase-matching geometry, this results in a unique signal direction making spatial isolation possible.

This response is a two-time interval correlation function of the polarizability:

$$R^{(5)}(\tau_2, \tau_4) = \left(\frac{i}{\hbar}\right)^2 \langle [[\alpha(\tau_2 + \tau_4), \alpha(\tau_2)], \alpha(0)]\rho_{eq}\rangle \quad (1)$$

where the square brackets denote commutators, the angled brackets denote an ensemble average, $\alpha(\tau)$ is the polarizability operator at time τ, and ρ_{eq} is the equilibrium density matrix. The origin of this signal depends on two primary components: any nonlinearity in the coordinate dependence of the polarizability[1] and any anharmonicity in the intermolecular modes.[9] Without at least one of these two sources, no fifth-order Raman signal can exist. It was expected that in most liquids each of these sources will contribute to the signal, and early work in the field indicated it should be possible to separate the effects of the two contributions.[10,11] Over the years, intense theoretical efforts have used a variety of approaches to simulate the fifth-order Raman response of various systems, including multimode Brownian oscillator models,[1,12,13] harmonic oscillator models,[14] normal-mode theory,[15−23] molecular dynamics simulations,[24−26] hydrodynamic theory,[27−31] the generalized Langevin equation,[32−34] classical time correlation functions,[35−37] and finite-field molecular dynamics simulations.[38−42] In several cases, this has required the development of new theories and computational approaches, with previous theories having proved inadequate at properly describing the liquid state. Collectively, the theoretical work in this area has demonstrated that the fifth-order Raman response is very sensitive to the details of the intermolecular potential and treatment of the liquid dynamics. Theoretical modeling of the response function has proved to be an important test bed for the accuracy of various theoretical approaches in treating liquid dynamics. On the basis of the sensitivity of the theoretical analyses, the fifth-order Raman experiment is arguably one of the most sensitive probes of the liquid state.

This high-order experiment is inherently a small signal experiment. The key rephasing pathway involves a Raman overtone that is orders of magnitude down in signal intensity from fundamental transitions of any given mode. This feature of the experiment has made the fifth-order Raman response function a great challenge to experimentalists. Apart from the small signal contributions, the experiment is complicated by the presence of cascaded third-order signals.[43−45] As discussed, the third-order field interaction is just the nuclear free-induction decay and does not access information on the time evolution of the bath coordinates. This signal contribution masked the key information of interest in the original experiments in the field.[46−52] The observations of these early experiments proved to be dominated by two cascaded third-order signals that produced a signal in the same phase-matching direction as the fifth-order response. It is only recently that a combination of phase-matching discrimination,[53] heterodyne detection,[54,55] and a cascade-suppressing polarization tensor element[39,56] has allowed the fifth-order response of liquid CS_2 to be successfully measured.[57] In this endeavor, the fifth-order response for CS_2 has been found to be exquisitely sensitive to the details of the sign of the nuclear response and position of nodes along the τ_4 probe axis.[24,39,58] Although the general features of the fifth-order response of CS_2 were similar in two separate reports,[54−58] there appeared to be conflicting reports from both experimental and theoretical studies of this interesting feature of the 2D spectrum. This issue has recently been clarified by comparing experiments that have both used the highly discriminating polarization configuration against cascades referred to as the Dutch Cross beam geometry.[56,59] In this configuration, signal contributions along the τ_2 pump direction previously observed[58] vanished and the two different experimental studies have converged on the fine details. For a more detailed review of the field please see ref 60.

The fifth-order Raman response of liquids constitutes an important proving ground for the advancement of both theory

and nonlinear spectroscopic methods in the study of liquids. This paper describes the extension of fifth-order Raman spectroscopy to the study of liquid benzene and further advances the prospects of using this approach to the general study of liquid dynamics.

2. Experimental Methods

The experimental procedure followed here is similar to our previous work with liquid CS_2.[53−57] A brief summary will be presented here. The laser source used in these experiments is a standard titanium:sapphire, regeneratively amplified femtosecond laser that produces 800 nm, 700 μJ, 100 femtosecond (fs) pulses at a 1 kHz repetition rate. A small fraction of this output is picked off and used as the 10 μJ, 800 nm probe beam, while for the two-color experiment the rest of the light is put through a 300 μm thick BBO doubling crystal, producing 120 μJ, 400 nm pulses which will be used as the pump pairs. Both the pump and probe beams are put through a pair of precompensation prisms to minimize pulse broadening effects of the intervening optics to the sample. The probe beam is then sequentially put through (1) a retroreflector mounted on a motorized, computer-controlled delay stage to control the probe time delay, τ_4, (2) a waveplate/polarizer combination for intensity control, (3) a waveplate to control the orientation of the probe polarization, and (4) a two-lens telescope to focus the beam into a 250 μm diameter spot on the diffractive optic that generates the phase-matching beam geometry. The pump beam is split into two equal beams using a beam splitter, producing the two pump arms. One pump beam is bounced off a retroreflector mounted on a motorized, computer-controlled translation stage to control the pump time delay, τ_2. The second beam is bounced off a retroreflector mounted on a manual translation stage which is used for coarse time-overlap adjustment. Each 400 nm beam is then put through its own version of the same sequence of optics as the probe beam. The result is three almost collinear beams, two blue and one near IR, focused onto the back surface of a transmission diffractive optic.[53]

The custom-made diffractive optical element (DOE) generates three exact replicas (two blue and one IR) of the required phase-matching beam geometry with slight horizontal separation between blue patterns and a large angular diffraction separating out the IR pattern. Using filters and irises, the proper beam geometry for the desired phase-matching conditions can be chosen. This results in two time-coincident blue beams generated by the manual translation stage arm, two time-coincident blue beams generated by the τ_2 motorized translation stage arm, and two time-coincident IR beams generated by the τ_4 motorized translation stage arm. One of the IR beams is generated by the diffractive optic so it overlaps perfectly with the phase-matched signal direction, which greatly facilitates alignment and allows for the possibility of heterodyne detection of the signal. The six beams are then reflected off two off-axis parabolic mirrors onto the sample cell. This has the effect of recreating the grating phase profile of the diffractive optic in the sample, ensuring that all phase-matching conditions are met. To avoid interaction between the beams in the glass of the diffractive optic, the laser pulses are kept temporally separated at the DOE. The pulses need to be time-overlapped at the sample, so glass is placed into the beam paths after the diffractive optic to delay the various pulses; fine control is obtained through tilting thin glass cover slips to precisely control the amount of glass each beam goes through. This allows the five beams to be time coincident at the sample. The signal alignment beam is then put through an iris followed by a polarizer to control the signal polarization, followed by a second iris to ensure complete isolation of the signal. Finally, a prism is used to separate off any scattered blue light from the IR signal and the beam is then focused onto a photodiode. A single pump beam is optically chopped after the diffractive optic, and a lock-in amplifier synchronized to the chopper is used to acquire the signal and transfer the signal output to a computer. A scan is performed by acquiring a signal at each position of either of the two motorized translation stages. In general, a raster scan is performed to acquire a full two-dimensional dataset where a τ_2 trace is taken with a data point per femtosecond; the τ_4 stage is then moved some small time increment (50 fs in this work), and τ_2 is rescanned. This procedure is repeated until the two-dimensional time region of interest is completed. A diagonal scan ($\tau_2 = \tau_4$) can be performed by scanning both translation stages simultaneously. The faster data acquisition permits this slice and other slices in the 2D spectrum to be collected with 1 fs time steps. The sample used is spectroscopic-grade benzene that is pumped through a flow cell with an optical path length of 400−500 μm using a peristaltic pump. The path length is controlled by using Teflon spacers of the desired thickness between the two compressed cell windows. The front window of the cell is a 100 μm thick microscope cover slip, kept thin so as to keep pulse broadening and group velocity mismatch problems to a minimum as the pulses enter the sample, and the back window is a 1 mm thick microscope slide for support. Since the index of refraction of the sample is different for the two laser wavelengths used, the pump and probe pulses have different velocities as they move through the cell. This can result in a time smearing that reduces the temporal resolution of the signal. To avoid this, sample path lengths are kept as short as possible while still maintaining a measurable signal.

TABLE 1: Wave-Vector Mismatch Values for the Direct Fifth-Order Process and Both Steps of the Cascaded Third-Order Processes in Liquid Benzene for the Crossed-Beam Phase-Matching Geometry[a]

process	Δk_a (cm^{-1})	Δk_b (cm^{-1})
direct	−17.866	
sequential 1	524.43	501.75
sequential 2	−461.91	441.99
parallel 1	1037.71	−1045.72
parallel 2	1037.71	−1045.72

[a] The subscripts a and b refer to the primary and secondary cascaded third-order processes, respectively, that generate a signal in the same signal direction as the desired fifth-order nuclear response.

Diffractive Optics. The advantages of diffractive optics are well-established: passively phase-locked laser pulses allow easy implementation of heterodyne detection,[54,55,61] more efficient focusing conditions due to the parallel electric fields of the diffracted beams,[61,62] simple alignment and signal detection,[53,63,64] and strict adherence to phase-matching conditions.[54,56] The custom diffractive optical element used here generates the *crossed-beam* phase-matching geometry which has excellent discrimination against the lower-order cascaded signals that have the potential to contaminate the signal.[43] The wave-vector mismatch numbers for both the direct and cascaded signals in liquid benzene using this geometry are given in Table 1 where the larger the $|\Delta k|$ value the further the process is from being perfectly phase matched and the greater the degree of discrimination (vide infra).

Heterodyne Detection. When signal intensity is measured, any phase information contained in the field is immediately lost. To retrieve this information, a reference field can be interfered with the signal field on the detector. This is called heterodyne

detection, and it allows full retrieval of the phase and amplitude of the signal field. In the case of a signal field, $E_{sig}(t)$, mixed with a reference field, $E_{ref}(t)$, the following expression is obtained:

$$I_{het}(t) = |E_{sig}(t) + E_{ref}(t)|^2 = |E_{sig}(t)|^2 + |E_{ref}(t)|^2 + 2E_{sig}(t)\,E_{ref}(t)\cos\Delta\phi \quad (2)$$

In this equation, $|E_{sig}(t)|^2$ is the signal intensity, or the homodyne signal measured when the reference field is blocked, and $|E_{ref}(t)|^2$ is the reference field intensity. The reference field intensity is generally a time-independent signal; however, because the reference can interact with the single chopped pump beam in the sample, a time-dependent signal can result along the probe delay. This pump-induced modulation of the reference (PIM) depends on the strength of the reference field which must be carefully controlled to try to minimize its contribution. The final term in the equation is the one of interest, since it contains the information about the signal field. We can control the phase of the measured signal by changing the relative phase of the signal and reference fields with respect to each other. This control over $\Delta\phi$ is obtained by placing a thin glass cover slip in the reference beam after the diffractive optic, before the sample. By rotating the angle of the cover slip, we control the relative phase of the reference with respect to the signal, allowing us to separate real and imaginary terms, pertinent to isolating the fifth-order signal of interest as described previously.[55] To properly account for all source terms in eq 2, three signals are measured for each time slice: (1) the signal with both the reference and probe unblocked (heterodyne signal), (2) the signal with the reference blocked and probe unblocked (homodyne signal), and (3) the signal with the probe blocked and reference unblocked (PIM). Signals 2 and 3 are then subtracted from signal 1 to obtain the signal field. In addition to the multiple time scans, we also cycle $\Delta\phi$ through a full π phase shift between the signal and reference fields. This allows us to see the change in phase of the various signal components, allowing us to identify the various contributions to the signal field. This is an important feature, since it is predicted that the cascaded signal will be phase-shifted from the fifth-order Raman signal.[55,65,66] The diffractive optic is key in this application, as it allows us to passively phase-lock the reference field to the signal field for this signal processing with a stability of $\lambda/50$ for periods of many hours.

Cascaded Signals. The simplest method of isolating the fifth-order signal from these contaminants is to ensure the phase-matching geometry chosen maximizes the fifth-order signal while minimizing the third-order signal. The two cascaded signals that must be accounted for are the *sequential* and *parallel* cascades (see Figure 2). The phase-matching requirement for the fifth-order signal is $\mathbf{k_s} = (\mathbf{k_1} - \mathbf{k_2}) - (\mathbf{k_3} - \mathbf{k_4}) + \mathbf{k_5}$; for the intermediate cascade steps, the equations are $\mathbf{k_{s1}} = \mathbf{k_2} - \mathbf{k_1} + \mathbf{k_3}$, $\mathbf{k_{s2}} = \mathbf{k_1} - \mathbf{k_2} + \mathbf{k_4}$, $\mathbf{k_{p1}} = \mathbf{k_1} - \mathbf{k_2} + \mathbf{k_5}$, and $\mathbf{k_{p2}} = \mathbf{k_4} - \mathbf{k_3} + \mathbf{k_5}$. This representation makes it clear that each cascaded signal is in fact a combination of two third-order Raman signals each of which is being generated in a skewed boxcar geometry, with the signal generated in one process acting as either a pump or probe field in the other. From these wave-vector equations, it is possible to calculate the phase mismatch for the cascaded processes using the experimental geometry (see Table 1). By increasing the mismatch for these processes while keeping the direct fifth-order process close to being perfectly phase matched, it is possible to strongly discriminate against the presence of any cascaded signals, preventing them from contaminating the experimentally measured response.

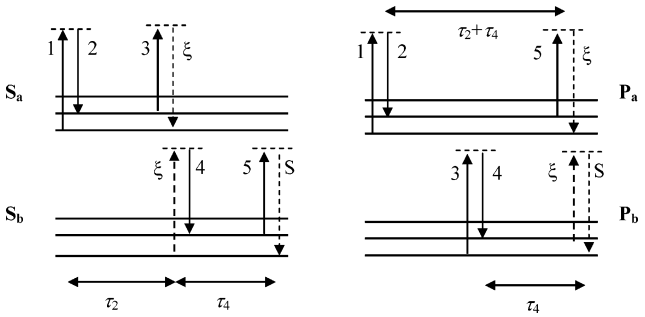

Figure 2. Energy level diagrams corresponding to the two different cascaded signal contributions in the fifth-order Raman experiment. $\mathbf{S_a}$ is the first sequential cascade step, $\mathbf{S_b}$ the second sequential cascade step, $\mathbf{P_a}$ is the first parallel cascade step, and $\mathbf{P_b}$ is the second parallel cascade step.

TABLE 2: Phase-Matching Coefficients for the Crossed-Beam Phase-Matching Geometry in Liquid Benzene with a 400 μm Sample Pathlength

process	Re $F(\Delta k, l)$	Im $F(\Delta k, l)$	$\lvert F(\Delta k, l)\rvert$
direct	0.9170	−0.3424	0.9789
sequential 1	−0.0005	0.0047	0.0048
sequential 2	0.0012	−0.0005	0.0013
parallel 1	0.0019	−0.0003	0.0019
parallel 2	0.0019	−0.0003	0.0019

In addition to the wave-vector mismatch, there are also other contributions such as path length and concentration that can affect the strength of the various signals.[65] Taking these factors into account and following the method established in ref 55, the following equations can be arrived at for the phase-matching factor $F(\Delta k, l)$:

$$|F(\Delta k, l)| = \sqrt{\text{Im } F^2 + \text{Re } F^2} \quad (3)$$

where

$$\text{Re } F(\Delta k, l) = \frac{\sin\left(\frac{\Delta k l}{2}\right)}{\frac{\Delta k l}{2}} \cos\left(\frac{\Delta k l}{2}\right) \quad (4)$$

$$\text{Im } F(\Delta k, l) = \frac{\sin\left(\frac{\Delta k l}{2}\right)}{\frac{\Delta k l}{2}} \sin\left(\frac{\Delta k l}{2}\right) \quad (5)$$

The results of these calculations for the experimental conditions are shown in Table 2. From them, it is evident that the fifth-order signal is almost perfectly phase matched while both cascaded signals have more than 2 orders of magnitude further discrimination. This level of suppression has proved to be sufficient to eliminate the presence of cascaded signals from the fifth-order signal of interest in liquid CS_2.[53−55]

3. Results

***$R^{(5)}_{zzzzzz}$* Response.** Previous attempts have been made to measure the fifth-order Raman response of benzene. One of the original fifth-order Raman experiments used benzene as a sample liquid, but the results were contaminated with cascaded signals.[46] The results for the heterodyne-detected all-parallel response, $R^{(5)}_{zzzzzz}$, and a 500 μm path length are shown in Figure 3. A two-dimensional dataset of the in-phase signal ($\Delta\phi \sim 0$) taken with a 400 μm sample pathlength is shown in Figure 4.

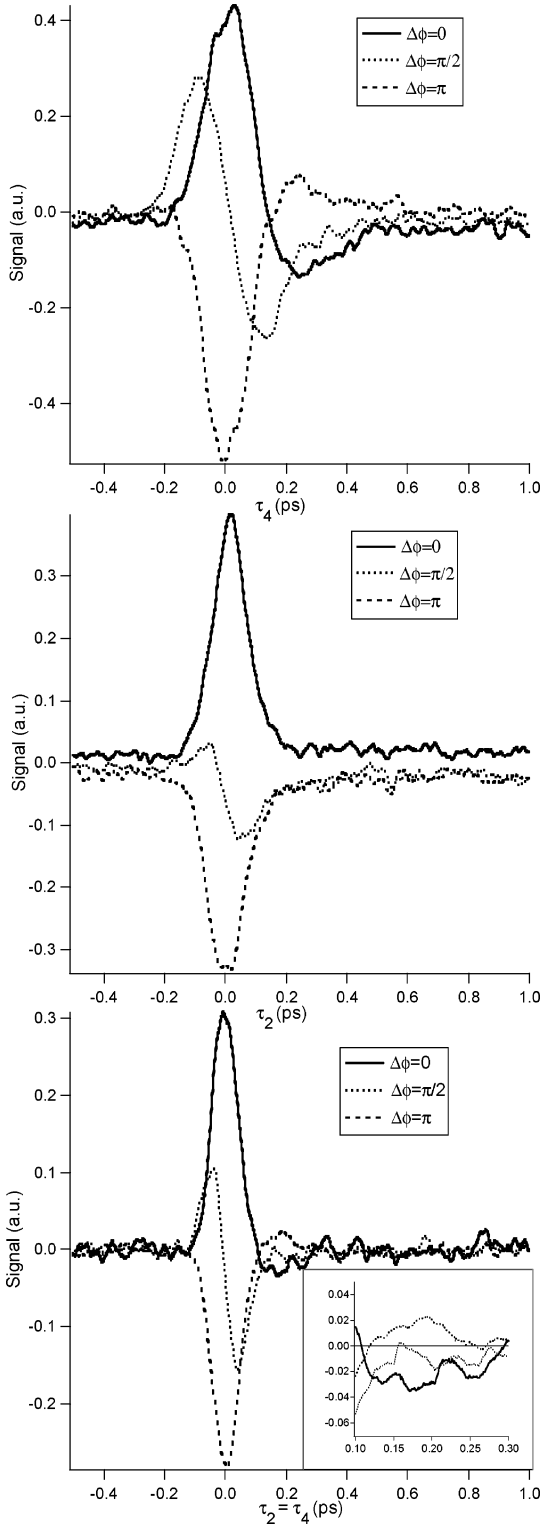

Figure 3. Heterodyne-detected fifth-order Raman response, $R^{(5)}_{zzzzzz}$, for liquid benzene using the crossed-beam phase-matching geometry and a 500 μm sample path length. Three relative phases are presented for three different time slices in the 2D spectrum: solid line ($\Delta\phi = 0$), dotted line ($\Delta\phi = \pi/2$), and dashed line ($\Delta\phi = \pi$). Note the inset of the diagonal scan shows a magnified section of the data to more clearly illustrate the diagonal nuclear rephasing signal.

Due to the long data acquisition time, this dataset was collected with coarser time steps and accompanying drifts in phase that leads to lower time resolution than in Figure 3. This figure provides the qualitative features of the full 2D spectrum. It should be noted that when the 5× increase in sample path length between the CS_2 and benzene experiments is taken into account and the same excitation conditions are used, the signal of liquid benzene is found to be 40 times smaller than that of liquid CS_2. Since we have no way of estimating the expected decrease in fifth-order signal amplitude between the two liquids, this information is provided merely for reference.

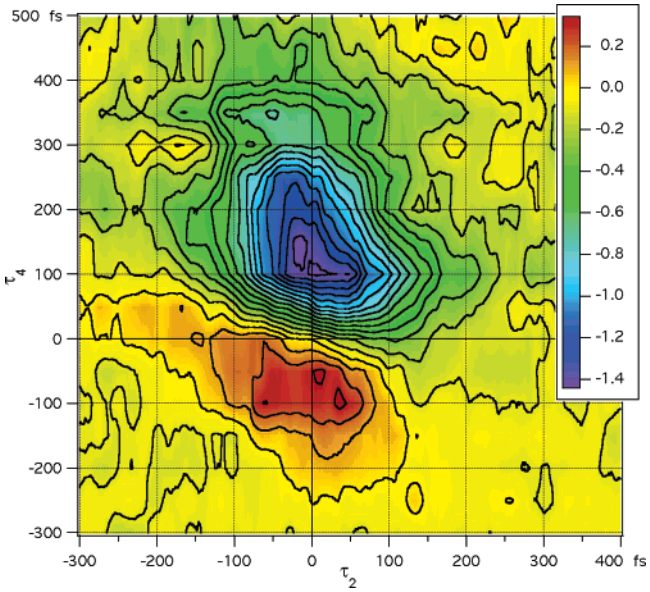

Figure 4. Heterodyne-detected fifth-order Raman response, $R^{(5)}_{zzzzzz}$, for liquid benzene using the crossed-beam phase-matching geometry and a 400 μm sample path length. The relative phase shown is $\Delta\phi \sim 0$. The signal consists of a ridge along τ_4 and shorter-lived off-axis components that give an L-like shape to the 2D spectrum.

The overall dynamics of the benzene signal are approximately similar to those of CS_2. The main features are a prominent ridge along the probe axis (τ_4), a very small short-lived signal along the time diagonal ($\tau_2 = \tau_4$), and no signal along the pump axis (τ_2). However, the specifics of several of the features are different. The signal along τ_4 shows a sign change in fashion similar to that seen in the liquid CS_2 Dutch Cross and $R^{(5)}_{yyzzzz}$ tensor elements but which is not seen in the all-parallel tensor element response of CS_2.[55,56] The time scale of this change in sign appears to indicate a change in phase between the electronic hyperpolarizability and the longer-lived nuclear contributions to the signal. In addition, the decay of the benzene signal along the probe axis is much faster than that of CS_2 (~500 fs compared to ~1.5 ps). This finding is in contrast to the nuclear free-induction decay that is very similar for the two liquids. The signal along the time diagonal is small, though definitely present, and only persists to ~300 fs. This rephasing time scale is longer than that in the $R^{(5)}_{zzzzzz}$ tensor element in CS_2 but substantially shorter and smaller in amplitude than that in the Dutch Cross tensor element where the CS_2 echo signal persists to ~400 fs.

Dutch Cross Response. The final experiment in determining the signal purity of the fifth-order Raman response is always the Dutch Cross tensor element. This tensor element uses a polarization angle of 60° between the two pumps and the probe/signal fields in both steps of the cascades which further suppresses the nuclear contribution to the cascaded signal by 10^4.[39,56] If the signal survives this polarization configuration, then it is deemed to be cascade free. This tensor element consists of setting the first pump pair polarization to a 60° angle counterclockwise, the second pump pair to 0°, and the probe/analyzer to 60° clockwise (all angles set looking downstream toward the sample). The response measured using this tensor

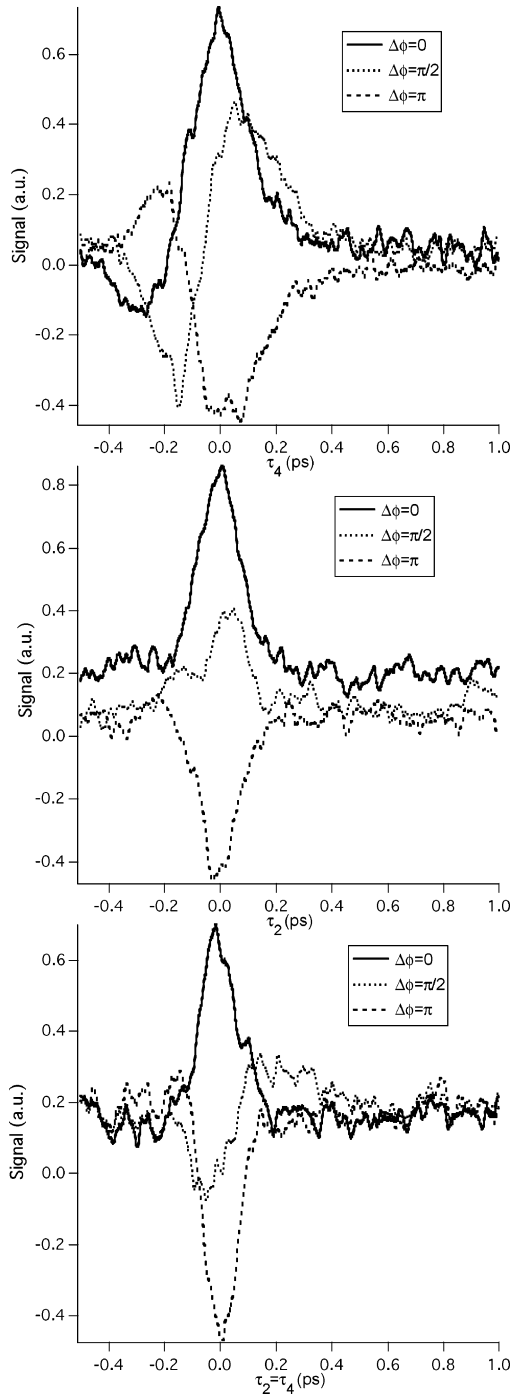

Figure 5. Heterodyne-detected fifth-order "Dutch Cross" Raman response for liquid benzene using the crossed-beam phase-matching geometry and a 400 μm sample path length. Three relative phases are presented for three different time slices: solid black line ($\Delta\phi = 0$), dotted line ($\Delta\phi = \pi/2$), and dashed line ($\Delta\phi = \pi$).

element and the crossed-beam geometry with a 400 μm sample path length of liquid benzene are shown in Figure 5.

The Dutch Cross response is approximately one-fifth the amplitude of the all-parallel response which made it difficult to measure within the decreased signal-to-noise ratio. The homodyne signal was almost below the measurement threshold, while the pump-induced modulation of the reference was of the same order of magnitude as the heterodyne signal. To improve the signal-to-noise ratio and eliminate any PIM contributions to the signal, the three contributions to eq 2 were each averaged over a minimum of five traces. This decrease in signal is approximately that expected when moving from $R^{(5)}_{zzzzzz}$ to a mixed-polarization tensor element.[55,67] Most importantly, the signal level is substantially larger than the potential 5 orders of magnitude drop expected for the nuclear cascaded signal.[39] The dynamics of the response remain identical to those of the all-parallel tensor element, though with a reduced electronic component at the time origin, as expected due to the crossed excitation pulse pairs. This result differs from that of liquid CS_2 where the Dutch Cross response introduced a phase shift between the electronic signal and the nuclear signal along the probe delay that was not present in the all-parallel tensor element. The fifth-order Raman response of liquid benzene shows comparatively the same dynamics for both the all-parallel and Dutch Cross tensor elements.

Finite-Field Molecular Dynamics Simulations. The third- and fifth-order Raman responses of liquid benzene were simulated using finite-field nonequilibrium molecular dynamics (FFMD).[38] The finite-field method essentially simulates the real experiment at a microscopic level: forces are applied in the simulation when pump pulses are applied in the experiment. The resultant susceptibility, $\chi^{(1)}$, that the probe experiences is calculated from the simulation when the probe pulse is applied in the experiment. Both lower- and higher-order unwanted contributions are eliminated by combining simulations where the polarization directions, *a* through *f* of the respective fields, are inverted, resulting in inversion of the force.[42] Note the reverse time ordering of the fields: *f* is the polarization of the first pump field and *a* the polarization of the signal. The inverted field is denoted $\bar{d}$. This procedure also strongly reduces noise in the simulated response. The third-order Raman response from the finite-field simulation is

$$R^{(3)}_{abcd}(t) = \frac{\chi^{(1)}_{ab;cd}(t) - \chi^{(1)}_{ab;c\bar{d}}(t)}{2E_cE_d\Delta t} \tag{6}$$

where E_c and E_d are the magnitudes of the applied pump fields and Δt is the time duration of the pump pulse. The equivalent expression for the FFMD fifth-order Raman response is

$$R^{(5)}_{abcdef}(\tau_2, \tau_4) = \frac{\chi^{(1)}_{ab;cd;ef}(\tau_2, \tau_4) + \chi^{(1)}_{ab;c\bar{d};e\bar{f}}(\tau_2, \tau_4) - \chi^{(1)}_{ab;c\bar{d};ef}(\tau_2, \tau_4) - \chi^{(1)}_{ab;cd;e\bar{f}}(\tau_2, \tau_4)}{4E_cE_dE_eE_f(\Delta t)^2} \tag{7}$$

This approach is equivalent to that of the time correlation function (TCF) method[16] in that the resulting response is identical. Performing the TCF calculation, however, requires the time-consuming evaluation of the stability matrix, whereas the FFMD simulation corresponds to calculating only one relevant vector of this matrix and is thus much faster. The third-order response has been calculated by several groups,[68−71] but this represents the first calculation of the fifth-order response.

All of the simulations were run with a slightly modified version of GROMACS 3.1.4.[39,72] The simulation box was prepared with 36 benzene molecules at 1 bar and 298 K. The single benzene molecules were kept rigid using three simulated atoms being placed at the apex of an equilateral triangle whose side lengths were fixed at 0.259 44 nm using the LINCS algorithm.[73] The mass and position of these atoms were selected to reproduce the overall mass, center of mass, and moment of inertia for the benzene molecule. Coulomb and Buckingham interaction forces exerted on the physical carbon and hydrogen atoms were transferred to the simulation atoms using the 3fd scheme of GROMACS. This procedure for simulating a rigid planar molecule is equivalent to the procedure for simulating a

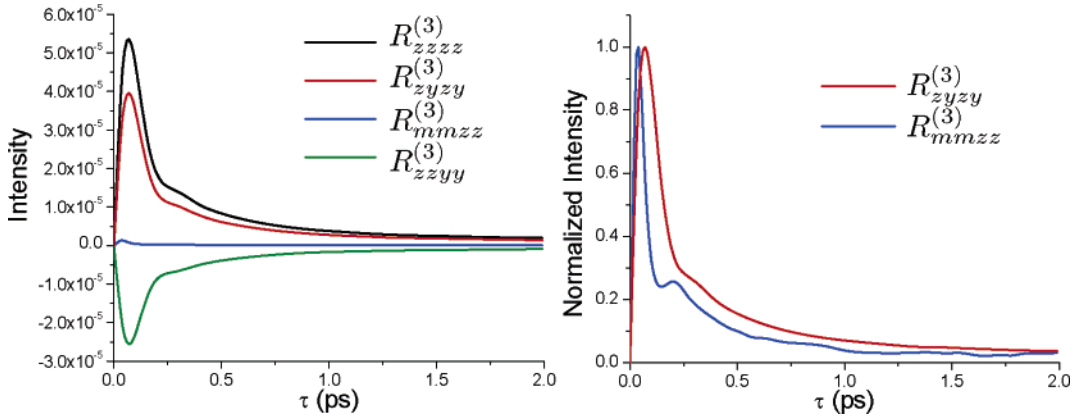

Figure 6. Calculated third-order Raman response of liquid benzene: (a) the tensor elements $R^{(3)}_{zzzz}$, $R^{(3)}_{yyzz}$, $R^{(3)}_{zyzy}$, and $R^{(3)}_{mmzz}$; (b) the normalized anisotropic, $R^{(3)}_{zyzy}$, and isotropic, $R^{(3)}_{mmzz}$, tensor elements.

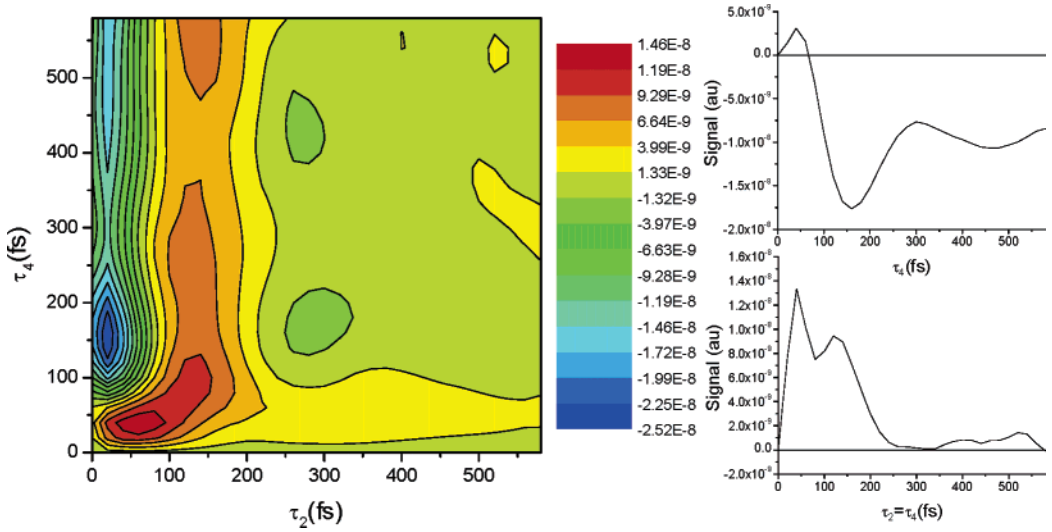

Figure 7. All-parallel fifth-order Raman response of liquid benzene calculated using the finite-field molecular dynamics method. Slices along the τ_4 probe axis ($\tau_2 = 0$) and the time diagonal ($\tau_2 = \tau_4$) are shown for further detail. Comparison should be made to the $\Delta\phi = 0$ data in Figure 3.

rigid linear molecule using two atoms.[38] The resulting dynamics are equivalent to that obtained with other schemes for rigid dynamics. Of course, the intramolecular dynamics are frozen, but this high-frequency motion can safely be neglected in the low-frequency part of the Raman response.[38] The charges and the parameters for the Buckingham potential were taken from a literature force field.[71,74] Keeping the molecules rigid allowed the simulation to be performed with 5 fs time steps. After 1 ns of equilibration, the density of the benzene liquid is found to be 0.9390 g/cm^3, slightly higher than the experimental value of 0.8765 g/cm^3.

In the present simulations, the dipole-induced dipole scheme[75] was employed for calculating the first-order susceptibilities and the forces exerted by the pulse pairs. A molecular polarizability was created at the center of mass using the direct reaction field scheme[40,76] by placing interacting polarizabilities on the three simulation atoms. The atomic polarizability on the simulation atoms was 3.184 549 Å^3, and the dipole screening factor 3.613 09 resulted in an overall molecular polarizability of 11.76 Å^3 along the axes in the plane of the ring and 7.09 Å^3 perpendicular to the ring.

The spectral simulations were performed in the microcanonical ensemble with electric field magnitudes of 4.21 V/nm applied during one 5 fs time step. The field strength was chosen to be strong enough to separate the signal from the noise and weak enough that higher-order response contributions could be neglected. This was ensured by performing initial investigations with varying field strengths. The third-order Raman response was calculated by averaging over 10 000 pairs of simulation trajectories with and without inverted polarization. Each trajectory had a duration of 2 ps. The calculated tensor elements of the third-order Raman response are shown in Figure 6. The calculated response functions are in very good agreement with earlier calculations[69,71] and experimental data.[77−79]

The anisotropic response, $R^{(3)}_{yzyz}$, rises fast and peaks at 100 fs. The rise is followed by a rapid decay, and at 250 fs, the response is at 25% of the peak value. A weak recurrence is observed between 250 and 500 fs. At longer times, the response function exhibits an exponential decay. Previous detailed analysis[68,71] showed that the response is dominated by reorientational motion; however, at short times, a considerable contribution from collective interaction-induced response is present.

The isotropic response, $R^{(3)}_{mmzz}$, where m denotes an axis forming a magic angle of 54.74° with the z-axis, has not been reported previously. It is much weaker than the anisotropic response. It shows two clear peaks. The first and most intense peak is seen at 50 fs, while the second is located at 200 fs. At longer times, the response function decays rapidly. Fluctuations beyond 1 ps are likely due to noise contributions affecting the extremely weak signal. The response functions $R^{(3)}_{zzzz}$ and $R^{(3)}_{yyzz}$

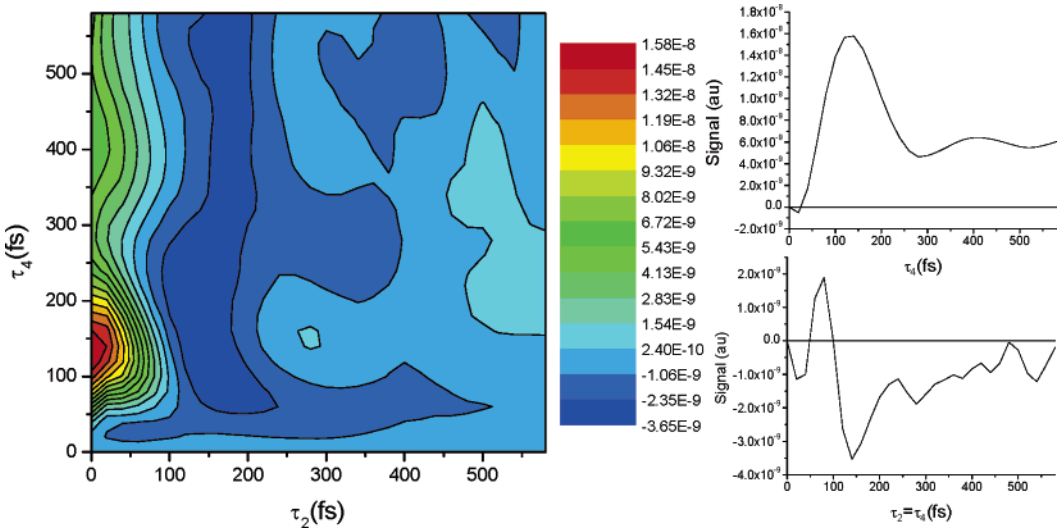

Figure 8. Dutch Cross fifth-order Raman response of liquid benzene calculated using the finite-field molecular dynamics method. Slices along the τ_4 probe axis ($\tau_2 = 0$) and the time diagonal ($\tau_2 = \tau_4$) are shown for further detail. Comparison should be made to the $\Delta\phi = 0$ data in Figure 5.

are shown as well, but these are given by linear combinations of the anisotropic and isotropic response functions and contain no further information.

The fifth-order Raman response was calculated by averaging over 2000 sets of simulation trajectories with the four different inverted polarization direction combinations. The time delays τ_2 and τ_4 were varied between 0 and 600 fs in steps of 10 fs. Two tensor elements were simulated: the all-parallel response, $R^{(5)}_{zzzzzz}$, and the Dutch Cross response.[39] The time slice where $\tau_2 = 0$ for $R^{(5)}_{zzzzzz}$ was extracted from the third-order calculation. For the Dutch Cross tensor element, this time slice was obtained from a calculation where the time step was reduced to 0.1 fs and τ_2 was set to 0.1 fs.

The fifth-order Raman responses for the all-parallel and Dutch Cross tensor elements are shown in Figures 7 and 8, respectively. The $R^{(5)}_{zzzzzz}$ response shows dynamics similar to those of the full molecular dynamics simulation of liquid carbon disulfide.[24,26] A positive peak is seen along the diagonal at $\tau_2 = \tau_4 \sim 50$ fs with a slight elongation along the pump axis (τ_2). A change in sign is observed along the probe axis at $\tau_4 = 60$ fs, and a strong negative peak is located close to the probe axis at $\tau_4 = 150$ fs. A negative ridge is seen along the τ_4-axis with a decay time longer than the simulation length of 600 fs. The signal along the time diagonal decays extremely rapidly and only persists to ~250 fs. The Dutch Cross response only has a significant signal along the probe axis. Along τ_4, a peak is seen at 125 fs and a much smaller peak is seen at 400 fs; in addition, the decay time of this signal exceeds the simulation length. When comparing the Dutch Cross tensor element with the experiment, caution is required. For this signal, the reorientational part of the response is strongly suppressed, which means it is more sensitive to interaction-induced effects than other tensor elements and therefore to the choice of force field and susceptibility model. Further calculations using more accurate interaction models are ongoing.

4. Discussion

The experimental results and the simulation results achieve reasonable agreement. For example, the overall dynamics of the FFMD all-parallel response is in good agreement with the experimental response. Both show a negative nuclear signal along the probe delay persisting to 500 fs and a complete lack of signal along the pump delay. The diagonal response of the simulation indicates a very short-lived signal that ends at 250 fs which matches the time scale of the experimental response decay but not the sign. The experimental response clearly shows the signal along the probe delay axis and the diagonal signal are the same sign, while the FFMD calculation indicates a change in sign. The FFMD simulation of the nuclear fifth-order response does not include any contribution from the electronic hyperpolarizability which is strongly present in the experimental signal around the time origin. From Figures 3 and 5, it is clear that this pulse-width-limited contribution is of opposite sign to that of the longer-lived nuclear fifth-order response. The combination of the limited time resolution of the experiment and this change in sign of the signal are interfering with resolving these very fast dynamics seen along the time diagonal in the FFMD simulations. The Dutch Cross FFMD simulation achieves better agreement in that its response only contains a signal along the probe delay and essentially no signal along the diagonal and the pump delay. This matches the experimental response quite well, with the only discrepancy lying in the decay rate of the signal along τ_4 which appears to be longer-lived in the simulation than the experiment. This behavior is also seen in the all-parallel tensor element. It should be noted that in both tensor elements the FFMD signal along the probe delay decays to less than 40% of its maximum value within 300 fs, and it is expected that noise contributions to the response will be larger at longer times. These simulation results are initial efforts, and further work will evaluate longer time dynamics, more accurate interaction models, and the validity of the simple molecular model chosen.

Much has been made of the presence of nodes in the molecular dynamics simulations of fifth-order Raman response of liquid CS_2 that are not present in the experimental response.[24,26] The presence of these nodes along the probe axis has been attributed to rotation−rotation coupling influencing the relative contributions to the signal of the intermolecular anharmonicity and the nonlinearity in the polarizability.[26] An analysis performed by Ma and Stratt on a single CS_2 molecule in a liquid xenon bath indicates that these nodes are a common feature and that they are highly sensitive to the details of the potential and experimental protocols; for example, the positions of the nodes are strongly influenced by the polarization tensor element chosen.[23,22] On the basis of their polarization analysis in comparison with both the experimental results and the MD

simulations, it appears possible that the MD simulation overestimates the contribution to the signal from the nonlinear dependence of the polarizability on coordinate. This is of concern because the response of liquid benzene also indicates the presence of nodes in both the experimental and simulated response. This possible overestimation will also affect the FFMD results for liquid benzene shown here, and may explain some of the previously noted discrepancies.

The principle components of the observed dynamics for the fifth-order response remain unchanged by the move from the all-parallel tensor element to the Dutch Cross tensor element. In both cases, the liquid appears to have little nuclear rephasing signal along the diagonal and a sign change between the electronic hyperpolarizability contribution at the time origin and the nuclear signal along the probe delay (τ_4). The signal along τ_4 contains information about the population dynamics of the Raman modes excited in the spectroscopy.[80] In liquid CS_2, this signal matches the free-induction decay (FID) of the third-order experiment.[55] In liquid benzene, this population relaxation occurs much more quickly than the free-induction decay of the third-order signal (see Figure 6). The echo signal along the time diagonal represents the inhomogeneous broadening contributions to the low-frequency line shape. In both liquid CS_2 and liquid benzene, there is little rephasing signal seen and thus little inhomogeneity indicated. The complication with this analysis is that in a homogeneously broadened liquid the dynamics of the rephasing signal should match the free-induction decay but the echo signal in both liquids is substantially faster than the corresponding FID. This raises the following question: is it possible the echo signal can be suppressed? In their initial work on CS_2, Saito and Ohmine determined that it was possible for the liquid modes to couple through the nonlinear polarizability.[16] This polarization quenching could potentially reduce the echo signal and affect its decay in the fifth-order response. A second possibility is that the overtone excited in this spectroscopy is unbound, or strongly damped such that rephasing really reports on the dynamics of the Raman overtone. If the excited intermolecular mode is sufficiently anharmonic, the harmonic approximation and level-independent dephasing in the Tanimura and Mukamel treatement breaks down. The overtone excitation will only act to effectively rephase the polarization during its decoherence time, and the measurement will be dominated by the faster loss of coherence in the overtone in relation to the fundamental 0−1 coherence. This latter mechanism to explain the fast decay in the signal along the diagonal is in some sense a distinct advantage, as the methodology would thereby preferentially probe the anharmonic features of the liquid potential energy surface. It is this feature that ultimately gives rise to the anharmonic motions of the constituent molecules that leads to the liquid state of the material. Unfortunately, liquid benzene is a poor candidate to explore these issues with respect to dephasing mechanisms of the bath memory, as little inhomogeneity is expected in its low-frequency spectrum. It will be important to investigate more structured liquids with stronger intermolecular forces, such as the hydrogen-bonded liquid formamide, to determine the impact of these possible echo-suppression pathways. The ultimate goal is to extend this spectroscopy to the study of liquid water.[12] The echo-suppression pathways diminish the signal along the rephasing direction that is most important to determining the long-range correlations in liquid water. It will be important to resolve the relative contribution polarization quenching makes to this signal feature in order to properly connect the signal to the microscopic correlations.[16] Combinations of MD and experiment should lead to a suitable resolution of this problem; the signal-to-noise ratio, however, needs to be improved to enable a sufficiently detailed comparison to experiment. This study will be particularly challenging for water in which the laser pulses will need to be dramatically reduced in pulse duration, and higher repetition rates and pulse energies will be needed to compensate for the expected much smaller signal for water than that of the present work.[24]

5. Conclusions

The fifth-order Raman response of liquid benzene has been successfully measured for the first time. The overall dynamics of the all-parallel and Dutch Cross tensor elements are very similar with a signal along the probe delay to 500 fs, a short-lived signal along the time diagonal to 300 fs, and no signal along the pump delay. The experimental response compares favorably with the results of a finite-field molecular dynamics simulation. The results indicate the low-frequency modes of liquid benzene are primarily homogeneously broadened with little to no inhomogeneous contributions. Benzene appears to behave as a liquid with little persistent structure on all experimentally accessible time scales. In addition, the signal appears to be dominated by the contributions from the anharmonicity of the intermolecular potential with little contribution from the nonlinear polarizability. This work represents an important step forward for fifth-order spectroscopy, as this is the first liquid to have divulged its fifth-order response outside of liquid carbon disulfide. The goal of the spectroscopy must now be focused on liquids with stronger intermolecular interactions, more structured liquids with the potential for longer-lived correlations and persistent memory of the structural heterogeneity of the liquid state.

Acknowledgment. This work was supported by the Natural Sciences and Engineering Research Council of Canada and Photonics Research Ontario. T.l.C.J. acknowledges the Netherlands Organization for Scientific Research (NWO) for support through a VENI grant.

References and Notes

(1) Tanimura, Y.; Mukamel, S. *J. Chem. Phys.* **1993**, *99*, 9496−9511.
(2) Loring, R. F.; Mukamel, S. *J. Chem. Phys.* **1985**, *83*, 2116−2128.
(3) Jonas, D. M. *Annu. Rev. Phys. Chem.* **2003**, *54*, 425−463.
(4) Bout, D. V.; Berg, M. *J. Raman Spectrosc.* **1995**, *26*, 503−511.
(5) Berg, M.; Vandenbout, D. A. *Acc. Chem. Res.* **1997**, *30*, 65−71.
(6) Kalpouzos, C.; Lotshaw, W. T.; McMorrow, D.; Kenney-Wallace, G. A. *J. Phys. Chem.* **1987**, *91*, 2028−2030.
(7) Ruhman, S.; Williams, L. R.; Joly, A. G.; Kohler, B.; Nelson, K. A. *J. Phys. Chem.* **1987**, *91*, 2237−2240.
(8) Lee, H. W. H.; Patterson, F. G.; Olson, R. W.; Wiersma, D. A.; Fayer, M. D. *Chem. Phys. Lett.* **1982**, *90*, 172−177.
(9) Tanimura, Y.; Okumura, K. *J. Chem. Phys.* **1997**, *106*, 2078−2095.
(10) Tanimura, Y. *Chem. Phys.* **1998**, *233*, 217−229.
(11) Tokmakoff, A.; Lang, M. J.; Jordanides, X. J.; Fleming, G. R. *Chem. Phys.* **1998**, *233*, 231−242.
(12) Palese, S.; Buontempo, J. T.; Schilling, L.; Lotshaw, W. T.; Tanimura, Y.; Mukamel, S.; Miller, R. J. D. *J. Phys. Chem.* **1994**, *98*, 12466−12470.
(13) Okumura, K.; Tanimura, Y. *J. Chem. Phys.* **1997**, *107*, 2267−2283.
(14) Steffen, T.; Fourkas, J. T.; Duppen, K. *J. Chem. Phys.* **1996**, *105*, 7364−7382.
(15) Ohmine, I.; Saito, S. *Acc. Chem. Res.* **1999**, *32*, 741−749.
(16) Saito, S.; Ohmine, I. *J. Chem. Phys.* **1998**, *108*, 240−251.
(17) Murry, R. L.; Fourkas, J. T.; Keyes, T. *J. Chem. Phys.* **1998**, *109*, 2814−2825.
(18) Murry, R. L.; Fourkas, J. T.; Keyes, T. *J. Chem. Phys.* **1998**, *109*, 7913−7922.
(19) Keyes, T.; Fourkas, J. T. *J. Chem. Phys.* **2000**, *112*, 287−293.
(20) Ma, A.; Stratt, R. M. *Phys. Rev. Lett.* **2000**, *85*, 1004−1007.
(21) Ma, A.; Stratt, R. M. *J. Chem. Phys.* **2002**, *116*, 4972−4984.
(22) Ma, A.; Stratt, R. M. *J. Chem. Phys.* **2003**, *119*, 8500−8510.

(23) Ma, A.; Stratt, R. M. *Bull. Korean Chem. Soc.* **2003**, *24*, 1126−1134.
(24) Saito, S.; Ohmine, I. *Phys. Rev. Lett.* **2002**, *88*, 207401.
(25) Ma, A.; Stratt, R. M. *J. Chem. Phys.* **2002**, *116*, 4962−4971.
(26) Saito, S.; Ohmine, I. *J. Chem. Phys.* **2003**, *119*, 9073−9087.
(27) Denny, R. A.; Reichman, D. R. *Phys. Rev. E* **2001**, *6306*, 065101.
(28) Denny, R. A.; Reichman, D. R. *J. Chem. Phys.* **2002**, *116*, 1979−1986.
(29) Denny, R. A.; Reichman, D. R. *J. Chem. Phys.* **2002**, *116*, 1987−1994.
(30) Cao, J. S.; Wu, J. L.; Yang, S. L. *J. Chem. Phys.* **2002**, *116*, 3739−3759.
(31) Cao, J. S.; Yang, S. L.; Wu, J. L. *J. Chem. Phys.* **2002**, *116*, 3760−3776.
(32) Van Zon, R.; Schofield, J. *Phys. Rev. E* **2002**, *65*, 011106.
(33) Van Zon, R.; Schofield, J. *Phys. Rev. E* **2002**, *65*, 011107.
(34) Kim, J.; Keyes, T. *Phys. Rev. E* **2002**, *65*, 061102.
(35) Devane, R.; Ridley, C.; Space, B.; Keyes, T. *J. Chem. Phys.* **2003**, *119*, 6073−6082.
(36) Devane, R.; Ridley, C.; Space, B.; Keyes, T. *Phys. Rev. E* **2004**, *70*, 050101.
(37) Devane, R.; Ridley, C.; Space, B.; Keyes, T. *J. Chem. Phys.* **2005**, *123*, 194507.
(38) Jansen, T. l. C.; Snijders, J. G.; Duppen, K. *J. Chem. Phys.* **2000**, *113*, 307−311.
(39) Jansen, T. l. C.; Snijders, J. G.; Duppen, K. *J. Chem. Phys.* **2001**, *114*, 10910−10921.
(40) Jansen, T. l. C.; Swart, M.; Jensen, L.; Van Duijnen, P. T.; Snijders, J. G.; Duppen, K. *J. Chem. Phys.* **2002**, *116*, 3277−3285.
(41) Jansen, T. l. C.; Duppen, K.; Snijders, J. G. *Bull. Korean Chem. Soc.* **2003**, *24*, 1102−1106.
(42) Jansen, T. l. C.; Duppen, K.; Snijders, J. G. *Phys. Rev. B* **2003**, *67*, 134206.
(43) Blank, D. A.; Kaufman, L. J.; Fleming, G. R. *J. Chem. Phys.* **1999**, *111*, 3105−3114.
(44) Kirkwood, J. C.; Ulness, D. J.; Albrecht, A. C.; Stimson, M. J. *Chem. Phys. Lett.* **1998**, *293*, 417−422.
(45) Ulness, D. J.; Kirkwood, J. C.; Albrecht, A. C. *J. Chem. Phys.* **1998**, *108*, 3897−3902.
(46) Steffen, T.; Duppen, K. *Phys. Rev. Lett.* **1996**, *76*, 1224−1227.
(47) Steffen, T.; Duppen, K. *J. Chem. Phys.* **1997**, *106*, 3854−3864.
(48) Tokmakoff, A.; Lang, M. J.; Larsen, D. S.; Fleming, G. R. *Chem. Phys. Lett.* **1997**, *272*, 48−54.
(49) Tokmakoff, A.; Lang, M. J.; Larsen, D. S.; Fleming, G. R.; Chernyak, V.; Mukamel, S. *Phys. Rev. Lett.* **1997**, *79*, 2702−2705.
(50) Tokmakoff, A.; Fleming, G. R. *J. Chem. Phys.* **1997**, *106*, 2569−2582.
(51) Tominaga, K.; Yoshihara, K. *Phys. Rev. Lett.* **1995**, *74*, 3061−3064.
(52) Tominaga, K.; Yoshihara, K. *J. Chem. Phys.* **1996**, *104*, 4419−4426.
(53) Astinov, V.; Kubarych, K. J.; Milne, C. J.; Miller, R. J. D. *Opt. Lett.* **2000**, *25*, 853−855.
(54) Astinov, V.; Kubarych, K. J.; Milne, C. J.; Miller, R. J. D. *Chem. Phys. Lett.* **2000**, *327*, 334−342.
(55) Kubarych, K. J.; Milne, C. J.; Lin, S.; Astinov, V.; Miller, R. J. D. *J. Chem. Phys.* **2002**, *116*, 2016−2042.
(56) Kubarych, K. J.; Milne, C. J.; Miller, R. J. D. *Chem. Phys. Lett.* **2003**, *369*, 635−642.
(57) Kubarych, K. J.; Milne, C. J.; Miller, R. J. D. *Int. Rev. Phys. Chem.* **2003**, *22*, 497−532.
(58) Kaufman, L. J.; Heo, J. Y.; Ziegler, L. D.; Fleming, G. R. *Phys. Rev. Lett.* **2002**, *88*, 207402.
(59) Kaufman, L.; Saito, S.; Ziegler, L.; Ohmine, I.; Fleming, G. Heterodyne detected fifth-order Nonresonant Raman Spectroscopy of CS_2: Evidence for Anharmonic Coupling. In *Ultrafast Phenomena XIII*; Miller, R., Murnane, M., Scherer, N., Weiner, A., Eds.; Springer: Berlin, 2003.
(60) Milne, C.; Li, Y.; Miller, R. Two-dimensional 5^{th}-order Raman spectroscopy: A new tool for the study of liquid-state dynamics. In *Time-resolved spectroscopy in complex liquids*; Torre, R., Ed.; Springer: Berlin, 2006.
(61) Goodno, G. D.; Dadusc, G.; Miller, R. J. D. *J. Opt. Soc. Am. B* **1998**, *15*, 1791−1794.
(62) Maznev, A. A.; Crimmins, T. F.; Nelson, K. A. *Opt. Lett.* **1998**, *23*, 1378−1380.
(63) Goodno, G. D.; Astinov, V.; Miller, R. J. D. *J. Phys. Chem. A* **1999**, *103*, 10630−10643.
(64) Goodno, G. D.; Miller, R. J. D. *J. Phys. Chem. A* **1999**, *103*, 10619−10629.
(65) Blank, D.; Fleming, G.; Cho, M.; Tokmakoff, A. Fifth Order Two-Dimensional Spectroscopy of the Intermolecular and Vibrational Dynamics in Liquids. In *Ultrafast Infrared and Raman spectroscopy*; Fayer, M. D., Ed.; Marcel Dekker: New York, 2001; Vol. 26.
(66) Golonzka, O.; Demirdoven, N.; Khalil, M.; Tokmakoff, A. *J. Chem. Phys.* **2000**, *113*, 9893−9896.
(67) Tokmakoff, A. *J. Chem. Phys.* **1996**, *105*, 13-21.
(68) Chelli, R.; Cardini, G.; Procacci, P.; Righini, R.; Califano, S.; Albrecht, A. *J. Chem. Phys.* **2000**, *113*, 6851−6863.
(69) Chelli, R.; Cardini, G.; Ricci, M.; Bartolini, P.; Righini, R.; Califano, S. *Phys. Chem. Chem. Phys.* **2001**, *3*, 2803−2810.
(70) Elola, M. D.; Ladanyi, B. M.; Scodinu, A.; Loughnane, B. J.; Fourkas, J. T. *J. Phys. Chem. B* **2005**, *109*, 24085−24099.
(71) Ryu, S.; Stratt, R. M. *J. Phys. Chem. B* **2004**, *108*, 6782−6795.
(72) Berendsen, H. J. C.; van der Spoel, D.; van Drunen, R. *Comput. Phys. Commun.* **1995**, *91*, 43−56.
(73) Hess, B.; Bekker, H.; Berendsen, H. J. C.; Fraaije, J. G. E. M. *J. Comput. Chem.* **1997**, *18*, 1463−1472.
(74) Williams, D. E.; Cox, S. R. *Acta Crystallogr., Sect. B* **1984**, *40*, 404−417.
(75) Geiger, L. C.; Ladanyi, B. M. *J. Chem. Phys.* **1987**, *87*, 191−202.
(76) Thole, B. T. *Chem. Phys.* **1981**, *59*, 341−350.
(77) Neelakandan, M.; Pant, D.; Quitevis, E. L. *J. Phys. Chem. A* **1997**, *101*, 2936−2945.
(78) Ricci, M.; Bartolini, P.; Chelli, R.; Cardini, G.; Califano, S.; Righini, R. *Phys. Chem. Chem. Phys.* **2001**, *3*, 2795−2802.
(79) Vöhringer, P.; Scherer, N. F. *J. Phys. Chem.* **1995**, *99*, 2684−2695.
(80) Steffen, T.; Duppen, K. *Chem. Phys.* **1998**, *233*, 267−285.